PHYSICAL REVIEW C **77**, 034307 (2008)

Nuclear ground-state spins and magnetic moments of ^{27}Mg, ^{29}Mg, and ^{31}Mg

M. Kowalska,[1,*] D. T. Yordanov,[2] K. Blaum,[1,3] P. Himpe,[2] P. Lievens,[4] S. Mallion,[2] R. Neugart,[1] G. Neyens,[2] and N. Vermeulen[2]

[1]*Institut für Physik, Universität Mainz, D-55099 Mainz, Germany*
[2]*Instituut voor Kern-en Stralingsfysica, Katholieke Universiteit Leuven, B-3001 Leuven, Belgium*
[3]*GSI, D-64291 Darmstadt, Germany*
[4]*Laboratorium voor Vaste-Stoffysica en Magnetisme, Katholieke Universiteit Leuven, B-3001 Leuven, Belgium*

(Received 2 January 2008; published 17 March 2008)

The ground-state spins and magnetic moments of neutron-rich ^{27}Mg, ^{29}Mg, and ^{31}Mg were measured for the first time with laser and β-NMR spectroscopy at ISOLDE/CERN. The hyperfine structure of ^{27}Mg—observed in fluorescence—confirms previous assignments of the spin $I = 1/2$ and reveals the magnetic moment $\mu_I(^{27}\mathrm{Mg}) = -0.4107(15)\,\mu_N$. The hyperfine structure and nuclear magnetic resonance of optically polarized ^{29}Mg—observed in the asymmetry of its β decay after implantation in a cubic crystal—give $I = 3/2$ and $\mu_I(^{29}\mathrm{Mg}) = +0.9780(6)\,\mu_N$. For ^{31}Mg they yield together $I = 1/2$ and $\mu_I(^{31}\mathrm{Mg}) = -0.88355(15)\,\mu_N$, where the negative magnetic moment provides evidence for a positive parity. The results for ^{27}Mg and ^{29}Mg agree well with shell-model calculations confined only to the sd model space, whereas the ground state of ^{31}Mg involves large contributions from neutrons in the pf shell, which places this nucleus inside the "island of inversion."

DOI: 10.1103/PhysRevC.77.034307 PACS number(s): 21.10.Ky, 21.10.Hw, 27.30.+t, 32.10.Fn

I. INTRODUCTION

The well-established shell model fails in some more exotic parts of the nuclear landscape where the shell gaps and magic numbers appear different from those close to stability. One such regions is the "island of inversion" located around $Z =$ 10–12 and the magic $N = 20$, where the nuclear ground states are much more deformed than expected for semi-magic nuclei. Such behavior can be explained by a collapse of the usual filling of the single-particle levels with neutrons occupying the pf shell before the lower sd shell is fully closed.

Neutron-rich Mg isotopes lie inside or at the borders of this "island." The experimental results prior to our investigations point to large ground-state deformations for the $^{31-34}$Mg isotopes, with 19 to 22 neutrons. Based on mass measurements [1,2] ^{31}Mg and ^{32}Mg are found too bound if $N = 20$ is assumed to be the neutron shell gap [3]. At the same time the first excited states in $^{31-34}$Mg lie unexpectedly below 1 MeV [4,5]. For ^{32}Mg and ^{34}Mg the reduced transition probability $B(E2)$ between this level and the ground state is also very large [5–8].

The existence of the "island of inversion" carries interesting questions related to its borders, physics mechanism, and its relation to other phenomena close to nuclear drip lines, such as changing magic numbers [9]. In spite of intensive experimental and theoretical studies, the answers to these questions are still not clear. The most probable mechanism driving the "island" involves shell gap weakening compared to typical sd shell nuclei. However, even when this is taken into account, there is disagreement among different calculations on which nuclei belong to this region, and whether its borders are gradual or abrupt.

This article presents the first experimental results on ground-state magnetic moments and directly measured spins of ^{27}Mg and ^{29}Mg. Furthermore, we present in detail our recent results concerning the spin and magnetic moment of ^{31}Mg [10], which provide direct evidence that this $N = 19$ nuclide lies inside the "island." Results for all three isotopes are discussed in the context of the shell model, with comparisons to several calculations made by using different recent residual interactions.

^{27}Mg, produced more abundantly than the other two isotopes, was studied with classical collinear laser spectroscopy by using fluorescence detection. The shorter lived ^{29}Mg and ^{31}Mg are well suited for β-asymmetry detected nuclear magnetic resonance (β-NMR) investigations with nuclear polarization achieved by optical pumping. The hyperfine structure observed in the β-decay asymmetry reveals the sign of the magnetic moments. The β-NMR resonances, visible as a decrease in the created nuclear polarization, reveal the nuclear g factors. After combining those with the hyperfine-structure results one can directly determine the nuclear spin [10].

II. EXPERIMENT

The experiments took place at the online isotope separator facility ISOLDE of CERN [11]. The Mg nuclei were produced by fragmentation of ^{238}U in a uranium carbide target under the impact of a 1.4-GeV proton beam, arriving every 1.2 s (or its multiple) in 2.5-μs bunches consisting at maximum of 3×10^{13} protons. After diffusion out of the target, the Mg atoms were selectively ionized with the laser ion source RILIS [12], accelerated to 60 keV, and guided through the general-purpose separator magnet GPS to our experimental setup. The Mg isotopes were investigated with a cw laser beam in the 279.635- and 280.353-nm transitions of singly charged ions from the ground $3s\ ^2S_{1/2}$ state to one of the two lowest excited $3p\ ^2P_{1/2,3/2}$ states (D_1 and D_2 lines).

---

[*] Present address: CERN, PH-Dept., 1211 Geneva 23, Switzerland.

The techniques used in the present work are based on the resonant interaction of ions and atoms in a fast beam with a geometrically superposed laser beam. In the case of β-NMR the resonant excitation is merely used for optical pumping and nuclear orientation via the hyperfine interaction. The collinear overlap between laser and ion and atom beams offers very favorable conditions, both for optical resonance detection and efficient optical pumping [13]. The primary advantage is a narrow Doppler width, a prerequisite of high resolution and sensitivity. For 60-keV Mg^+ ions with an energy spread of 1.5 eV[1] this means a Doppler width of only about 30 MHz, which is comparable to the 41-MHz natural line width of the D_1 and D_2 transitions in Mg^+. The small Doppler broadening is also crucial during optical pumping, where it ensures that most of the atoms are excited and polarized by the laser light fixed at resonance frequency.

An additional useful feature of the collinear method is the possibility to scan across optical resonances by adjusting the beam velocity with a tunable acceleration voltage. Owing to the Doppler effect, the ions "see" a laser frequency ν shifted from the frequency in the laboratory frame ν_{las}. For co-propagating beams, the relation between ν and ν_{las} can be expressed by

$$\nu_{\text{las}} = \nu \frac{1+\beta}{\sqrt{1-\beta^2}}, \tag{1}$$

with $\beta = \sqrt{1-(1+eU/mc^2)^{-2}} \approx \sqrt{2eU/mc^2}$. Here U is the accelerating voltage and m the rest mass of the ion.

The experimental setup using this configuration is presented schematically in Fig. 1. The ion beam of interest is guided into the apparatus via an electrostatic deflector, so that it can be overlapped with the laser light, which enters straight through a quartz window. After passing ion-optical elements the beam reaches the section where it is post-accelerated with a tunable voltage of maximum ±10 kV applied in steps to four cylindrical electrodes.

This part is followed by a 20-cm-long charge-exchange cell containing sodium vapor and put at the post-acceleration potential of the last cylindrical electrode. Charge-exchange neutralization is used for an experiment on ^8Li serving as a reference for NMR studies, in which case the potential at the charge-exchange cell determines the atom velocity downstream. For spectroscopy of Mg^+ ions the charge-exchange cell is not heated. In this case, the ion velocity is controlled by the potential at the excitation region insulated from both sides by thick plastic flanges. A voltage offset compared to the charge-exchange cell ensures that the ions are not optically pumped to "dark" states before entering the detection region, which is especially important for fluorescence detection. The last part of the apparatus, used only for β-decay detection, hosts the implantation crystal surrounded by the NMR coil. Thin scintillation detectors and the poles of the 0.3-T NMR magnet are placed outside the vacuum chamber.

A. Laser system

The cw laser system consists of an Ar^+ laser (Coherent Innova 400) pumping at 6 W in the multiline visible mode (mainly 488 and 514 nm) a ring dye laser (Coherent 699-21). The ring output is around 100–200 mW at 670 nm (with DCM dye as active medium) for reference β-NMR measurements on ^8Li and 0.5–1 W at 560 nm (with Pyrromethene 556 dye) for Mg^+. In the latter case the light is additionally frequency-doubled in an external cavity (Spectra-Physics Wavetrain) with angle phase matching and BBO as the nonlinear crystal. With 5–10% doubling efficiency, up to 20–50 mW of UV light at 280 nm is available. For optical pumping on average 10 mW is guided into the setup, whereas for fluorescence detection even 1 mW of UV is sufficient.

B. Optical detection

For measurements using optical detection, the laser light is linearly polarized and the entrance window is set at Brewster's angle to minimize the reflection losses and the background from scattered light. The detection of resonances takes place in the first 20 cm of the insulated region, where the fluorescence light is reflected on one side by a cylindrical mirror, and on the other side a 1:1 image of the beam is created on the front windows of two photomultipliers with the help of converging lenses. In this configuration for both studied transitions in Mg^+ we reach on average an overall efficiency of 1 detected

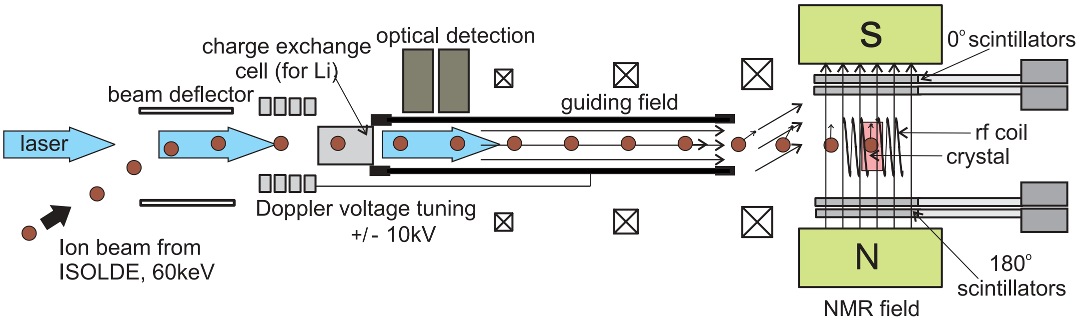

FIG. 1. (Color online) Collinear laser spectroscopy and β-NMR setup.

---

[1] This is the typical energy spread from the ISOLDE UC_x target and laser ion source, derived from the width of the Doppler component of Mg^+ optical resonances fitted with the Voigt profile (i.e., a convolution of the Doppler and Lorentz profiles).

photon in 15,000 ions delivered by ISOLDE,[2] compared to the background of around 3000 photons per second for the typical laser intensity of 1 mW, which causes negligible power broadening of the D_1 and D_2 lines in Mg^+.

C. Beta-decay asymmetry detection

In the case of β-asymmetry detection, the laser light is a tool to create nuclear spin polarization, defined as $P_I = \langle m_I \rangle / I$. This is achieved by the optical pumping process in which circularly polarized light polarizes the total atomic angular momenta F by inducing transitions between the m_F magnetic sublevels of the ground-state and excited-state hyperfine multiplets [14]. The same ion interacts with many photons, which subsequently transfer their angular momentum. As a result, the ion is in the ground-state sublevel with maximum $m_F = +F$ if σ^+ light polarization is used (or in the minimum $m_F = -F$ for σ^- polarization). The theoretical 100% polarization is lowered by the hyperfine pumping, in which the excited state decays to the other ground-state F level, which cannot be excited by the same laser frequency.

The circular polarization is created by a UV polarizer and a quarter-wave plate. In this configuration the light enters the vacuum apparatus by a quartz window placed perpendicular to the beam direction. The optical pumping takes place in the whole isolated section. The quantization axis for σ^+ or σ^- resonance absorption is established by a small ($B \approx 0.5$ mT) longitudinal magnetic field, shielded from external magnetic fields by a μ-metal foil. Next, the ions reach the fringe field of a 0.3-T NMR magnet—with field lines perpendicular to the beam direction—where rotation and subsequent adiabatic decoupling of the nuclear and electron spins takes place. The latter is shown schematically in the Breit-Rabi diagram of Fig. 2 for the example of $^{29}\mathrm{Mg}$.

The ions are finally implanted into a suitable crystal placed in the center of the magnet and β-decay electrons are detected in two pairs of thin plastic scintillators, placed at 0 and 180 degrees with respect to the magnetic field. When the ions are in resonance with the laser light, the spins are polarized, and the intensity of the emitted β particles is anisotropic in space with their angular distribution $W_\beta(\theta)$ given by

$$W_\beta(\theta) = 1 + a_\beta \, (v/c) \, P_I \, \cos\theta. \tag{2}$$

Here a_β is the β-decay asymmetry parameter depending on the spin change in the decay, θ is the angle between the direction of particle emission and the magnetic field, and v is the velocity of the decay electrons. The observed quantity is the experimental asymmetry $A_{\mathrm{exp}} = [N(0^\circ) - N(180^\circ)]/[N(0^\circ) + N(180^\circ)]$, where $N(0^\circ)$ and $N(180^\circ)$ represent coincident β counts in the two scintillators of both detectors.

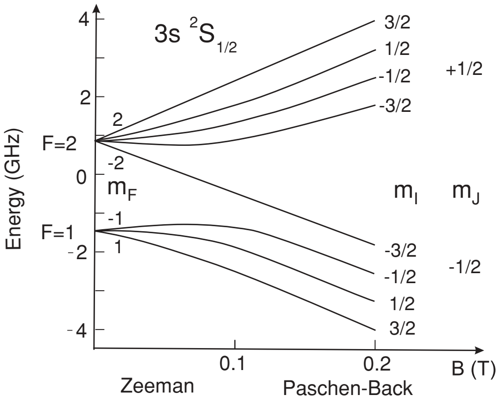

FIG. 2. Adiabatic decoupling of the nuclear and electronic spins in a magnetic field for the example of $^{29}\mathrm{Mg}$ ($I = 3/2$, $\mu_I > 0$).

In the case of hyperfine structure measurements, the β-decay asymmetry is observed as a function of the voltage applied to the optical pumping region. For NMR studies, however, the voltage is set at the hyperfine-structure component giving the highest β asymmetry, and a tunable radio-frequency field, perpendicular to the static magnetic field, is applied to the implantation crystal. This oscillating field is generated by an rf current flowing through a coil placed around the host crystal. To obtain a sufficiently high rf field strength, the signal from the rf generator passes through a broadband amplifier and a tunable resonant LC circuit.

III. RESULTS

To the first order, the energy shift caused by the hyperfine interaction between atomic electrons with total angular momentum J and a nucleus with spin I is connected to the magnetic dipole moment μ_I and the electric quadrupole moment Q of the nucleus by

$$E_F = \frac{1}{2} A K + B \, \frac{\frac{3}{4} K(K+1) - I(I+1)J(J+1)}{2I(2I-1)J(2J-1)}. \tag{3}$$

Here $F = |I - J|, \ldots, I + J$ stands for the total angular momentum and $K = F(F+1) - I(I+1) - J(J+1)$. The hyperfine structure parameters A and B are proportional, respectively, to μ_I and Q.[3] In the following, we are interested in μ_I, which can be derived from the A factor of a particular isotope if the corresponding A factor is also measured for an isotope with a known magnetic moment μ_{ref}:

$$\mu_I = \mu_{\mathrm{ref}} \, \frac{A \, I}{A_{\mathrm{ref}} I_{\mathrm{ref}}}. \tag{4}$$

One neglects corrections from the finite charge and magnetization distribution of the nucleus, which for Mg are of the order of 10^{-3} [15]. We fit the recorded hyperfine structure spectra with Lorentz or Voigt line profiles of independent amplitudes, common width, and positions related by Eq. (3).

The electromagnetic moments of nuclei can also be derived from NMR measurements. Since in cubic host crystals there is no electric field gradient at regular lattice sites, the quadrupole interaction energy is zero, and the Zeeman energy of a nucleus

---

[2] This efficiency takes into account beam losses of about 50% from the limited acceptance of our setup.

[3] The B factor for the studied transitions in Mg^+ is much smaller than the A factor.

with spin I in a strong magnetic field B_0 is given by

$$E(m_I) = -m_I(\mu_I/I)B_0 = -m_I g_I B_0 \mu_N = -m_I\, h\, \nu_L, \quad (5)$$

where m_I is the magnetic quantum number, g_I is the nuclear g factor, and ν_L is the Larmor frequency.

A radio-frequency field at frequency ν_L induces transitions between Zeeman levels, which for short-lived nuclei can be observed as NMR resonances in the β-decay asymmetry. By recording the NMR signal of the isotope of interest and of a reference isotope of the same chemical element with known μ_{ref}, one can determine the unknown g factor by using the relation

$$|g_I| = |g_{\text{ref}}| \frac{\nu_L}{\nu_{\text{ref}}} \quad (6)$$

and the magnetic moment $\mu_I = g_I I \mu_N$. If the reference is a nucleus of a different chemical element, Eq. (6) has to include additionally the diamagnetic corrections [16] to account for different shielding of the external magnetic field by the atomic electrons.

If the spin of a given nucleus cannot be determined from the hyperfine structure alone, it is derived unambiguously by combining information from the hyperfine structure and NMR. For the splitting between the $J = 1/2$ ground-state sublevels $F = I + 1/2$ and $F' = I - 1/2$ one obtains $\Delta E = A(I + 1/2)$, where the A factor can be expressed in g_I and the ratio A/g_I known for the reference isotope, yielding

$$I = \frac{\Delta E}{g_I} \frac{g_{\text{ref}}}{A_{\text{ref}}} - 1/2. \quad (7)$$

The parity of the ground state can be deduced in some cases from the sign of the magnetic moment, which in the single-particle model—where the levels have pure configurations—is different for nuclear levels with total angular momentum $l - 1/2$ and $l + 1/2$ (where l is the orbital angular momentum). The sign is usually not changed in the many-particle approach where different configurations can mix, but in ambiguous cases one may have to rely on comparing the measured magnetic moment with theoretical predictions.

A. Optical pumping simulations

To predict the hyperfine structure pattern observed in β decay, we performed simulations of the optical pumping process [17]. These were based on the semiclassical approach and weak-field approximation [18], where the latter allows us to use first-order perturbation theory. This leaves the population of the excited-state sublevels very small compared to the ground-state ones, and thus the temporal evolution of level occupation can be described with atomic rate equations,

$$\frac{d}{dt} N_i = \sum_j P_{ij}^{\text{st}}(\nu)\,(M_j - N_i) + \sum_j P_{ij}^{\text{sp}} M_j, \quad (8)$$

$$\frac{d}{dt} M_j = \sum_i P_{ij}^{\text{st}}(\nu)\,(N_i - M_j) - \sum_i P_{ij}^{\text{sp}} M_j, \quad (9)$$

where P_{ij}^{sp} and P_{ij}^{st} are the probabilities of spontaneous and stimulated transitions, respectively, and N_i and M_j represent populations of all m_F substates in the ground state and in the excited state, respectively.

The probability for spontaneous emission P_{ij}^{sp} is equal to the Einstein coefficient A_{ij} and can be derived from the lifetime τ of the excited $P_{1/2,\,3/2}$ states by using the Wigner $3j$ and $6j$ symbols [19],

$$P_{ij}^{\text{sp}} = A_{ij} = \frac{D}{\tau} \begin{Bmatrix} J & F & I \\ F' & J' & 1 \end{Bmatrix}^2 \begin{pmatrix} F & 1 & F' \\ m_F & \Delta m_F & -m'_F \end{pmatrix}^2, \quad (10)$$

with $D = (2F + 1)(2F' + 1)(2J + 1)$. Here J, F represent the ground state and J', F' the excited state, and $\Delta m_F = m'_F - m_F$.

The probabilities of stimulated emission and absorption are the product of the incident photon flux and the optical cross section, where the latter depends on the Einstein coefficient for stimulated transitions, $B_{ij} = A_{ij}\, c^3/(8\pi h \nu^3)$, and on the absorption profile [18]. By assuming a narrow-band incident laser light of frequency ν and power density ρ, these probabilities become

$$P_{ij}^{\text{st}} = \left(\frac{c}{2\pi\nu}\right)^3 \rho\, \frac{A_{ij}}{2h\tau} \frac{1}{(\nu_{ij} - \nu)^2 + [1/(4\pi\tau)]^2}, \quad (11)$$

where ν_{ij} is the resonance frequency. The absorption profile is assumed to be Lorentzian with the width being the natural width, governed only by the lifetime τ of the excited state. Power and Doppler broadening, leading, respectively, to an increase of the Lorentz width and a contribution from a Gaussian profile, are not included, because both simplifications do not interfere with the excellent description of the spectra.

After solving the coupled differential equations numerically (with the Runge-Kutta algorithm [20]) we obtain populations of all involved magnetic substates m_F at a chosen moment of time. The adiabatic decoupling in the transitional field to the NMR magnet means a movement along the levels of the Breit-Rabi diagram (Fig. 2) from the $|F, m_F\rangle$ to the $|m_J, m_I\rangle$ regime. Therefore, from the occupation numbers obtained for the coupled system, we obtain the populations of the corresponding m_I for the decoupled case and we can calculate the nuclear spin polarization P_I, which determines the β-decay asymmetry observed in the experiment.

These rate equations were used to predict the shape of the β-asymmetry spectra, as well as to perform least-squares fits to the available data on ^{29}Mg and ^{31}Mg.

B. Hyperfine structure of the reference ^{25}Mg

The hyperfine structure of ^{25}Mg was used as a reference for all hyperfine structure measurements. Its resonances were detected optically in the D_1 and D_2 transitions. From these, the A-factor values were found for all involved atomic levels of ^{25}Mg, as presented in Table I. $A(^2S_{1/2})$ agrees well with the precise literature value $A(^{25}\text{Mg}, {}^2S_{1/2}) = -596.254376(54)$ MHz [21], which is used further as a reference for Eq. (4), together with the known magnetic moment $\mu_I(^{25}\text{Mg}) = -0.85545(8)\,\mu_N$ [16]. The A factors of the excited levels, as well as $B(^2P_{3/2}) = +24.4(10)$ MHz, have been measured for the first time.

TABLE I. Measured hyperfine structure A factors for ^{25,27,29,31}Mg, with the confirmed tabulated spin values [22] and the new $I = 1/2$ for ^{31}Mg [10] (in MHz) assumed.

Isotope	Spin	$A(^2S_{1/2})$	$A(^2P_{1/2})$	$A(^2P_{3/2})$
^{25}Mg	5/2	−596.5(3)	−102.7(4)	−18.7(3)
^{27}Mg	1/2	−1431(5)	−253(6)	–
^{29}Mg	3/2	+1130(5)[a]	–	+35(2)[a]
^{31}Mg	1/2	−3082(4)	−530(7)	−95.2(14)

[a] The uncertainty accounts for the unresolved quadrupole interaction by assuming a possible range $|B(^2P_{3/2})| < 20$ MHz.

C. Hyperfine structure and magnetic moment of ^{27}Mg

^{27}Mg was studied with optical detection in the D_1 transition. With the ISOLDE production yield of about 10^8 ions per second we observed three hyperfine components (Fig. 3), which confirms the indirect spin assignment, $I = 1/2$, from the literature [22]. The relative position of the resonances furthermore corresponds to a negative magnetic moment. (For positive μ_I one would obtain a mirror image of the presented structure.)

Based on three independent data sets the average ground-state A factor is $A(^{27}\mathrm{Mg}, ^2\mathrm{S}_{1/2}) = -1431(5)$ MHz (Table I). Using Eq. (4) and ^{25}Mg as the reference, we obtain $g_I(^{27}\mathrm{Mg}) = -0.8214(30)$ and $\mu_I(^{27}\mathrm{Mg}) = -0.4107(15)\,\mu_N$.

D. Hyperfine structure and magnetic moment of ^{29}Mg

The studies on ^{29}Mg, with a production yield of about 6×10^6 ions/s, were performed by using β-decay detection on an implanted sample. We chose a cubic MgO host lattice, since this gives a longer relaxation time (around 500 ms) and higher average asymmetry than other tested crystals (see Ref. [23]). However, the maximum observed β-decay asymmetry for ^{29}Mg was only 2%. This is in agreement with the small asymmetry parameter $a_\beta = 15\%$ [see Eq. (2)] calculated by using the known branching ratios [22] and assuming a pure Gamow-Teller transition. Furthermore, the hyperfine pumping for nuclei with spin $I = 3/2$ lowers the attainable polarization P_I below 40%, and the 1.3-s half-life of ^{29}Mg is almost three times the relaxation time in MgO; thus a substantial part of the decaying nuclei is unpolarized and contributes to an isotropic background.

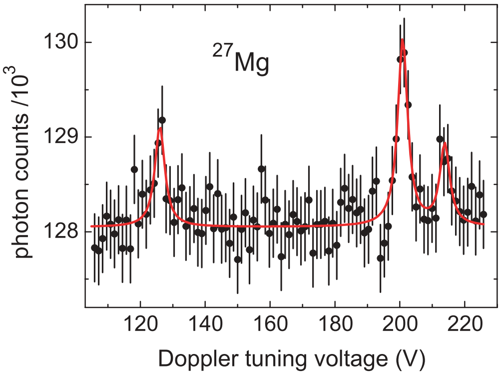

FIG. 3. (Color online) Hyperfine structure of the D_1 transition in ^{27}Mg.

In Fig. 4, next to the experimental hyperfine structure, we present results of the simulations described in Sec. III A, performed for spin $I = 3/2$ and a positive magnetic moment. These simulations take into account the asymmetry parameter, half-life, relaxation time, as well as the solid angle of detection, and a one-second observation time. The agreement in relative amplitudes and positions of different hyperfine components with respect to the center of gravity of the hyperfine multiplet is very good. This confirms the spin and reveals the sign of the magnetic moment to be positive. Also the absolute amplitudes are comparable, with the largest asymmetry expected at 3.5% and reaching 2% in reality.

The ^{29}Mg A factors derived from the hyperfine structure are presented in Table I. The resolution and statistics are insufficient to derive the B factor; therefore in the fits B was varied between −20 and 20 MHz, which increases the uncertainty of the A factors. Using again $A(^2S_{1/2})$ and Eq. (4), one obtains $g_I(^{29}\mathrm{Mg}) = +0.649(3)$. In a second step of the experiment, the β-NMR method is employed to reduce considerably the uncertainty of the g factor. For this purpose the acceleration voltage was set to the highest peak, corresponding to the $|F = 2\rangle \to |F' = 3\rangle$ transition with σ^+ laser polarization. The NMR measurements were performed with an rf-field amplitude of about 50 μT, corresponding to about 0.25 A for the rf current flowing through the resonance coil. This allowed us to nearly saturate the NMR transitions and to record spectra such as the one shown in Fig. 5.

A weighted average of two independent measurements yields the Larmor frequency $\nu_L(^{29}\mathrm{Mg}) = 1424.1(9)$ kHz. Within 24 hours from the measurements on ^{29}Mg we recorded β-NMR signals for the reference nucleus ^{8}Li, whose resonance was found at $\nu_L(^8\mathrm{Li}) = 1806.932(13)$ kHz, based on a weighted average of four independent spectra. Equation (6) with the known $g_I(^8\mathrm{Li}) = +0.826780(9)$ [16] and diamagnetic corrections for Mg and Li (respectively, 1.0007322 and 1.0001048 [16]) yields $g_I(^{29}\mathrm{Mg}) = +0.6520(4)$, where the systematic uncertainties are negligible. The positive sign of g_I is determined by the relative position of peaks in the hyperfine structure. The derived g_I agrees with the less precise result from the hyperfine splitting. With the spin confirmed to be $I = 3/2$, $\mu_I(^{29}\mathrm{Mg}) = +0.9780(6)\,\mu_N$.

E. Magnetic moment and spin of ^{31}Mg

^{31}Mg was also investigated using hyperfine structure studies by β-asymmetry detection, as well as by β-NMR measurements. On average 1.5×10^5 ions/s were delivered by ISOLDE and implanted in the MgO crystal, where decay asymmetries up to 7% were observed. In Fig. 6 we compare the measured hyperfine structure spectrum for the D_2 transition with the simulated one. The latter—similarly as for ^{29}Mg—takes into account the relaxation time, the solid angle of detection, and observation time (750 ms), with unknown asymmetry parameter $|a_\beta|$ set to 100%. To reproduce the observed patterns, the sign of a_β has to be negative. The positions, relative amplitudes, and signs of all observed resonances are

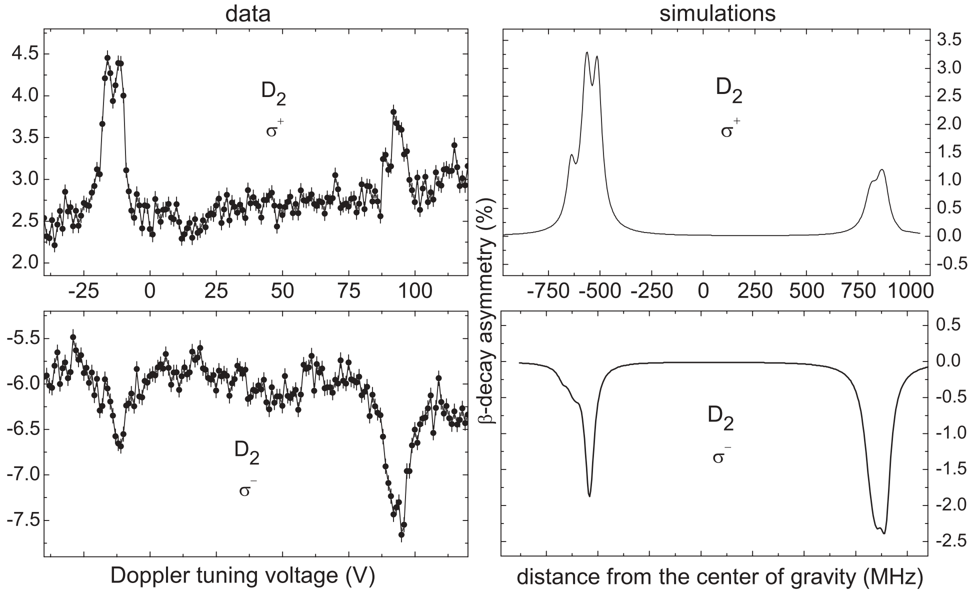

FIG. 4. Measured hyperfine structure (left) and simulations (right) for the D_2 transition in ^{29}Mg ($I = 3/2, \mu_I > 0$). The simulated spectra are given on a frequency scale that corresponds to the voltage scale in the real spectra. The experimental baseline is different from zero because of an instrumental asymmetry offset.

very well reproduced by the simulations for $I = 1/2$, whereas they are in clear disagreement with predictions for other spins (see, e.g., simulations for spin 3/2 in Fig. 4). Also, the measured asymmetry a factor of 5–6 lower than the predicted one; thus the asymmetry factor $|a_\beta|$ has to be larger than 20%.

The NMR measurement was performed with the acceleration voltage set at the strongest, 7%-asymmetry component. We used rf-field amplitudes of around 30 μT, corresponding to a 0.15-A current in the coil. The analysis of a dozen independent spectra gives the average Larmor frequency $\nu_L(^{31}\mathrm{Mg}) = 3859.65(15)$ kHz.[4] By using the same ^{8}Li reference Larmor frequency as for ^{29}Mg, $\nu_L(^8\mathrm{Li}) = 1806.932(13)$ kHz, together with diamagnetic corrections [16] for Li and Mg, the absolute value of the g factor becomes $|g_I(^{31}\mathrm{Mg})| = 1.7671(3)$. The final error includes the systematic contribution accounting for a possible magnetic field drift between the measurements on ^{31}Mg and ^{8}Li and the uncertainty in the beam positions on the crystal.

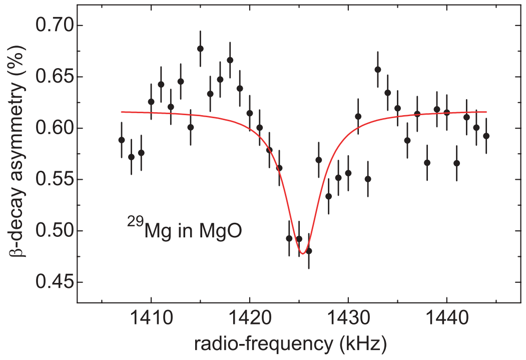

FIG. 5. (Color online) Larmor resonance of ^{29}Mg in MgO.

The nuclear spin can be unambiguously determined by combing both measurements. For this, we use in Eq. (7) the measured ground-state splitting of ^{31}Mg, $\Delta E = -3082(4)$ MHz, and the reference data for ^{25}Mg. In this way we obtain $I = 1/2$, which confirms the preliminary assignment based only on the hyperfine structure. Furthermore, the hyperfine structure pattern clearly corresponds to a negative A factor, and thus $\mu_I(^{31}\mathrm{Mg}) = -0.88355(15)\,\mu_N$ [10].

IV. DISCUSSION

For the discussion of our experimental results summarized in Table II, we first compare them to the single-particle approach characterized by pure one-nucleon configurations and magnetic moments known as Schmidt values [15]. Next, we use several many-particle shell-model approaches, which all treat ^{16}O as an inert core. The first shell-model calculation is based on the "universal" *sd* residual interaction USD [24] and its most recent update USDB [25]. Both interactions are tailored to the *sd*-shell nuclei and restrict valence neutrons and protons to this major shell. These calculations were performed by us with the shell-model code ANTOINE [26], which uses the conventional direct diagonalization of the Hamiltonian in the full valence space.

The other approaches were developed especially for the "island of inversion." They allow valence protons and neutrons into the full *sd* shell and part of the *pf*-shell orbits. To lower the "intruder" configurations with nucleons in the *pf* shell in

TABLE II. Ground-state spins and magnetic moments measured in the present work.

Isotope	I	μ_I (μ_N)
^{27}Mg	1/2	−0.4107(15)
^{29}Mg	3/2	+0.9780(6)
^{31}Mg	1/2	−0.88355(15)

---

[4] This reevaluation of the available data, which also takes into account a systematic frequency shift, resulted in Larmor frequencies slightly smaller than the ones in Ref. [10], however without influencing the deduced value for the magnetic moment.

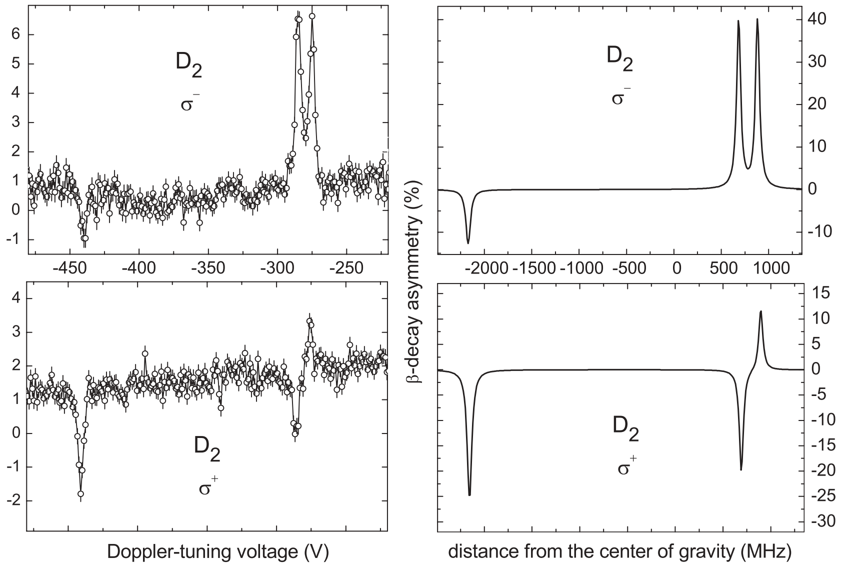

FIG. 6. Measured hyperfine structure (left) and its simulations (right) for the D_2 transition in ^{31}Mg ($I = 1/2, \mu_I < 0, a_\beta = -1$). The simulated spectra are given on a frequency scale that corresponds to the voltage scale in the real spectra. The experimental baseline is different from zero because of an instrumental asymmetry offset.

energy they assume a smaller $N = 20$ shell gap and increased proton-neutron correlations [27]. For the *sd* part, they all use the matrix elements from USD. However, they differ in the cross-shell and *pf*-shell matrix elements and in the way of diagonalizing the Hamiltonian. The first set of calculations, performed with the ANTOINE code, is based on the residual interaction known as SDPF.SM or iokin.spdf.si35 [27–29] and developed by the Madrid-Strasbourg group. Its model space consists of full *sd* and *pf* shells, but constraints on the number of particles and number of occupied orbits in the *pf* shell are necessary to make the calculations possible. Here, the results for ^{31}Mg are reported from Nowacki [30]. Minor modifications to SDPF.SM lead to the interaction SDPF.NR [31] with the results for ^{31}Mg taken from Ref. [32]. The second group of calculations uses residual interactions developed by the Tokyo group, SDPF-M [33] and its modification SDPF-M′, which has different *pf* matrix elements [34], with a sd-$p_{3/2}f_{7/2}$ model space. They are based on the Monte Carlo shell model (MCSM) [35], which uses the quantum Monte Carlo method to include only bases important for a specific eigenstate, which are then diagonalized. In this way it can include more possible configurations. All calculations with SDPF-M or SDPF-M′ were performed for us by the Tokyo group [10,36,37].[5] The main difference between the Mardid-Strasbourg and Tokyo interactions, except for model space and the diagonalization method, is the fact that the latter predict a larger $N = 16$ and smaller $N = 20$ shell gaps, which makes them produce an enlarged "island of inversion" and enhanced proton-neutron correlations [27].

All presented calculations were performed with free-nucleon *g* factors. This choice was based on studies of other nuclei in this region (see, e.g., Ref. [39]) and arguments pointed out by Brown and Wildenthal [24]. Since the Tokyo group usually uses effective values for SDPF-M and SDPF-M′ [40], we present their results with both effective- and free-nucleon *g* factors.

A. Magnetic moment of ^{27}Mg

In the single-particle shell model the ground state of ^{27}Mg is formed by four protons in the $d_{5/2}$ orbit coupled to spin 0 and one neutron in the $s_{1/2}$ orbit with spin-parity $1/2^+$, to which corresponds a Schmidt value of $-1.91\ \mu_N$. Our result of spin 1/2 agrees with this assignment, points to a positive parity, and confirms the spin-parity reported before [22]. However, the measured μ_I is far from the single-particle value and agrees with it only in sign.

The magnetic moment of ^{27}Mg is slightly smaller than those of its even-Z isotones, but they can be all explained well by our USD shell-model calculations (Fig. 7). However, there is no clear improvement when using the updated interaction, USDB, the agreement being better for some isotones, but worse for others. The neutron $(d_{5/2})^6 s_{1/2}$ configuration is dominant in

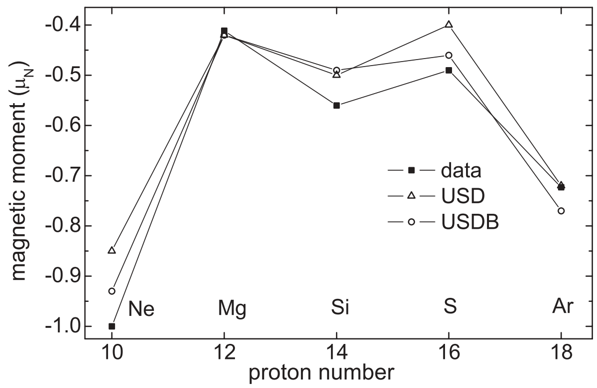

FIG. 7. Theoretical and experimental magnetic moments of $N = 15$ isotones with even Z. Theoretical values based on our calculations using USD [24] and USDB [25] residual interactions and the ANTOINE code [26]. Experimental values are from Refs. [16,41,42] and this work.

---

[5] The SDPF-M′ used in the present work is different from another small modification of SDPF-M also labeled SDPF-M′, which has been used recently to understand the large *g* factor of ^{34}Al [38].

the ground states of all nuclei considered in Fig. 7, although it varies from 30% in ^{27}Mg, ^{29}Si, and ^{31}S to 50% in ^{25}Ne and ^{33}Ar.

B. Magnetic moment of ^{29}Mg

In the single-particle picture the ground-state properties of ^{29}Mg should be governed by one unpaired neutron in the $d_{3/2}$ shell. This implies $I^\pi = 3/2^+$, which agrees with our measured spin and the spin-parity reported in the literature [22]. The corresponding Schmidt value, $+1.146\,\mu_N$, is close to the measured value. However, the agreement is not perfect, which indicates that configuration mixing plays a role.

In Fig. 8 we plot the magnetic moments of ^{29}Mg and other nuclei with even Z and one unpaired neutron (or hole) in the $d_{3/2}$ shell (i.e., $N = 17$ or 19). The experimental results for ^{29}Mg and all the $N = 19$ isotones are close to the Schmidt value, whereas the other $N = 17$ isotones have smaller magnetic moments. Our calculations using the USD interaction reproduce well these experimental data. They also show that the expected single-particle neutron configuration accounts for 80% of the ground-state wave function in $N = 19$ isotones and for around 50% in $N = 17$ isotones. In the case of ^{29}Mg these additional admixtures are different from those in ^{33}S and ^{35}Ar, hence explaining the difference in their magnetic moments. Surprisingly, the agreement is generally worse for the recent USDB interaction, which overestimates all presented moments. Figure 9 shows the experimental and theoretical energies, spins, and parities for several lowest lying levels in ^{29}Mg, as well as the predicted g factors for the lowest $1/2^+$ and $3/2^+$ states. We find the $3/2^+$ level as the ground state with USDB and at 50 keV with USD. This is also the case for calculations of the Tokyo group, SDPF-M, which included mixing and allowed up to five neutrons into $p_{3/2}$ and $f_{7/2}$ orbits, as well as for the Madrid-Strasbourg interaction SDPF.SM, where we obtained the intruder states by blocking one or two neutrons in the full pf shell. Also the calculated g factors agree rather well with the experimental value, with deviations smaller than 10% and with best agreement found for the Madrid-Strasbourg interaction.

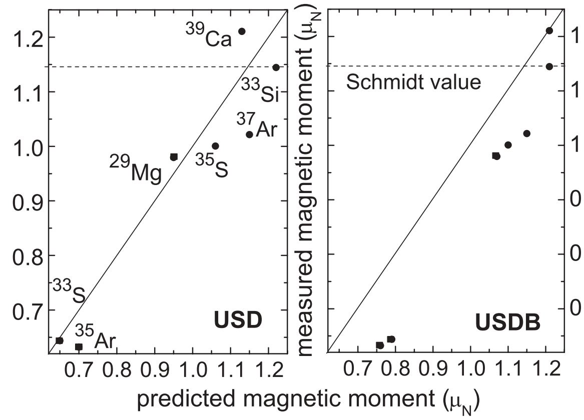

FIG. 8. Theoretical and experimental magnetic moments of even-Z, odd-N nuclei with one unpaired neutron in the $d_{3/2}$ shell ($N = 17$ or 19) from Refs. [16,41,43,44] and our measurements.

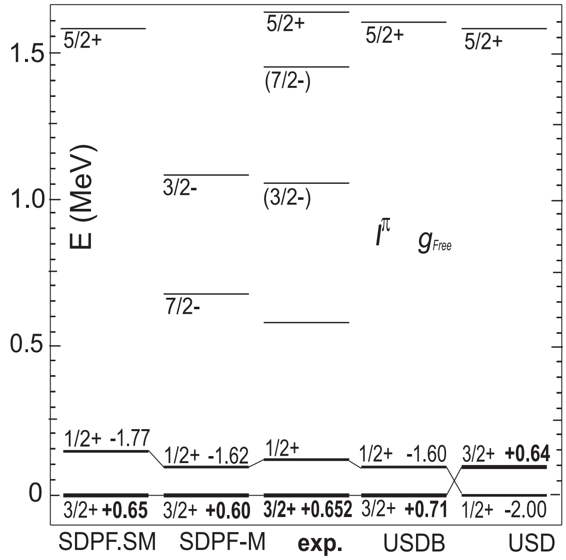

FIG. 9. Measured and predicted excitation energies and g factors for the ground state and lowest excited states in ^{29}Mg. Experimental results are from Ref. [45] and our measurements. Theoretical values from our own calculations and Ref. [37].

This comparison shows firmly that the ground state of ^{29}Mg can be described very well with existing residual interactions by using only the sd shell and free-nucleon g factors. Thus, this nucleus lies clearly outside the "island of inversion."

C. Magnetic moment and spin of ^{31}Mg

For the more exotic ^{31}Mg the extreme single-particle predictions are the same as for ^{29}Mg, since they are based on one unpaired neutron in the $d_{3/2}$ orbit. However, our measured $I = 1/2$ excludes this simple picture. One possible explanation for this difference would be that the state we measure is not the ground state but a long-lived isomer, but β- and γ- decay studies [46] have excluded the possibility of such a long-lived state in ^{31}Mg. The ground-state spin 1/2 can also explain the derived negative sign of the asymmetry factor a_β: With $I = 1/2$ the measured branching ratios in the decay of ^{31}Mg to the excited states of ^{31}Al together with shell-model spin assignments in ^{31}Al [32] give $a_\beta \approx -25\%$.

There are several possible explanations for the unexpected spin 1/2 of the ground state, even if one assumes only neutron excitations, since the large $d_{5/2}$-$s_{1/2}$ proton gap justifies neglecting proton excitations. The first obvious candidate is the positive-parity neutron configuration $s_{1/2}(d_{3/2})^4$, which is the only way to stay within the sd shell. All other possibilities involve promotion of neutrons to the pf shell, such as the configuration $(s_{1/2})^2 d_{3/2}(f_{7/2})^2$. To decide which scenario is correct and what is the parity of the ground state, we compare the measured excitation energies and g factors to theory (Fig. 10).

Our calculations with USD and USDB interactions, which restrict valence neutrons to the sd shell, cannot reproduce the observed $I = 1/2$ level as the ground state, and not even as a low-lying state. The lowest $I = 1/2$ state appears only at

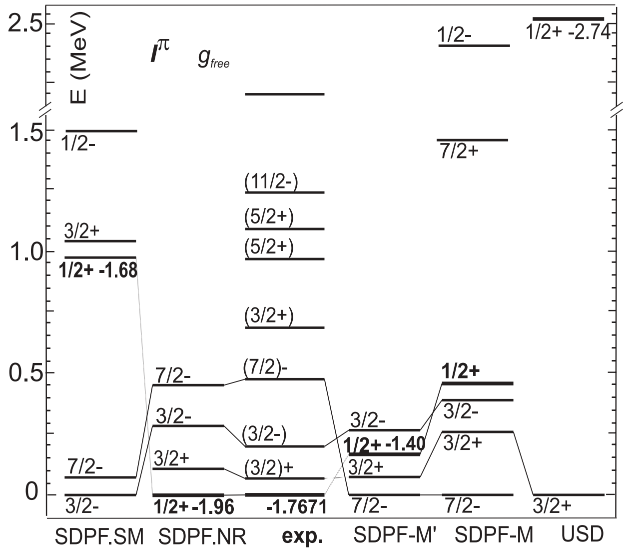

FIG. 10. Measured and predicted excitation energies, spins, parities, and g factors for the ground state and lowest excited states in ^{31}Mg. For the pf-shell calculations intruder $1/2^-$ states are also shown. For the SDPF.NR interaction only levels up to 500 keV are shown. Experimental results are from Refs. [46,47] and our measurements. Theoretical results are from the present calculations and Refs. [10,32,36,37].

2.5 MeV. It has positive parity and corresponds to the $s_{1/2}(d_{3/2})^4$ configuration with a g factor exceeding the measured value by more than 50%. However, all interactions that allow neutrons into pf-shell orbits give predictions of the level scheme and the g factor of the lowest 1/2 state much closer to the experimental data. For the Madrid-Strasbourg calculations with one or two neutrons blocked in the full sd-pf space and no mixing between 0p-0h and 2p-2h configurations, the first 1/2 state appears at about 1 MeV excitation energy. It represents a 2p-2h state of positive parity and has $g_I = -1.68$. At the same time, the 0p-0h level appears at as high as 2.7 MeV, whereas the lowest $1/2^-$ level is predicted around 1.5 MeV with a positive magnetic moment. The situation is even better for the Tokyo interaction SDPF-M with up to seven neutrons in the $p_{3/2}f_{7/2}$ orbits and mixing between normal and intruder p-h configurations. It predicts the lowest 1/2 level at only 0.5 MeV with positive parity and the g factor equal to -1.70 (or -1.32 with effective g_I), composed of 2p-2h configurations to about 96%. The sd-only $1/2^+$ state is predicted to be much higher, whereas the first 1/2 level of negative parity, with a 96% contribution of 1p-1h configurations, appears at 2.4 MeV with a positive magnetic moment, similar as in the Madrid-Strasbourg calculations. The same calculation with the newer Tokyo interaction SPDF-M′ gives the best agreement with the experimental energies, since the 2p-2h $1/2^+$ state goes down to 0.3 MeV. This is due to a stronger pairing matrix element within the pf shell, which leads to a gain in energy for the 2p-2h states with respect to the 1p-1h states. However, the predicted g factor of -1.4 (or -1.2 with effective g factors) is somewhat too small. These calculations show that the measured ground state of ^{31}Mg has positive parity and an almost pure 2p-2h wave function. Furthermore, earlier β-decay experiments already assigned a positive parity to the ground state, based on the fact that it is populated by the β decay from the positive-parity ground state of ^{31}Na [47].

Although both types of pf-shell calculations predict pf intruder states below sd-only configurations and give g factors very close to our result, the negative-parity 1p-1h states are still lower in energy than the observed $1/2^+$ ground state. So far, there exists only one calculation in full agreement with the experiment [32]; it uses the new Madrid-Strasbourg SDPF.NR interaction [31] and includes sd-$f_{7/2}p_{3/2}$ neutron orbits (Fig. 10). SDPF.NR is a modification of SDPF.SM, aimed at describing the best ^{31}Mg states without changing the description of some neighboring nuclei, such as ^{33}Mg and ^{35}Si. The fact that it yields a $1/2^+$ ground state with $g_I = -1.97$ is a very positive result, but it remains to be seen whether it can predict properly the forthcoming results in and around the "island," such as the spin and g factor of ^{33}Mg [48], which also indicate an almost pure 2p-2h ground state, or the large g factor of ^{34}Al [38], which suggests a reduction not only of $N = 20$ but also of the $N = 28$ shell gap. However, even with the open question as to how to predict the $I = 1/2^+$ state below negative-parity configurations, it is clear that ^{31}Mg has a purely intruder ground state and hence belongs to the "island of inversion."

In terms of a collective model, the rich low-energy spectrum of ^{31}Mg clearly suggests a deformed ground state, in which a neutron hole is coupled to a deformed core of ^{32}Mg ($N = 20$). In the Nilsson shell model, a $1/2^+$ ground state for $N = 19$ corresponds to a $1/2^+[200]$ configuration coming from the $d_{3/2}$ spherical orbit, above the $1/2^-[330]$ orbit from the spherical $f_{7/2}$ state. A calculation with a harmonic oscillator potential shows that the $K = 1/2^+$ orbit crosses $K = 1/2^-$ only for a deformation parameter $\beta \approx 0.4$ [32], which means that the ground state of ^{31}Mg is very deformed. The experimental g factor of the $1/2^+$ state is reproduced extremely well for a very large deformation parameter, $\beta \approx 0.5$, yielding $g_I = -1.78$ [32]. Maréchal *et al.* [32] also calculated g factors of other low-lying states in this nucleus and found a very good agreement with the shell-model calculations using the Madrid-Strasbourd SDPF.SM interaction. This result supports the interpretation of the ground state of ^{31}Mg being a well-deformed structure resulting from promotion of neutrons across the sd-pf shell gap. Very recently another calculation using this approach has been published where harmonic oscillator potentials have been substituted with Woods-Saxon potentials [49], which should be better suited for nuclei with weakly bound neutrons. The depth of the potential was chosen so that the spin and parities of the ground states of ^{31}Mg and ^{33}Mg as measured by us [10,48] are obtained for $\beta \approx 0.5$. The calculation shows that the ground-state deformation is caused by a near degeneracy of the $d_{5/2}$-$s_{1/2}$ and $f_{7/2}$-$p_{3/2}$ levels in the spherical potential, whereas the disappearance of $N = 20$ is related to the properties of weakly bound states with low orbital angular momentum, in particular $l = 0, 1$.

^{31}Mg has been recently studied theoretically with a different approach, namely the antisymmetrized molecular dynamics (AMD) plus generator coordinate method (GCM) with the Gogny D1S effective nucleon-nucleon interaction [50], which addressed both the positive- and negative-parity states, as well as the coexistence of many-particle and many-hole states. The calculations [51] reproduce the spin and parity of the ground state, explain it by a pure 2p-2h configuration, and give a magnetic moment of $-0.91\,\mu_N$, which is close to our experimental value. Furthermore, they predict a rich low-energy spectrum and agree with our spin-parity assignments for the lowest levels [10].

V. CONCLUSION

The hyperfine structure of ^{27}Mg studied with collinear laser spectroscopy and optical detection confirmed the previous spin assignment and revealed a magnetic moment whose value and sign are comparable to those of the even-Z, $N = 15$ isotones and agree very well with many-particle calculations within the sd shell. Investigations of the shorter lived ^{29}Mg, whose hyperfine structure and NMR signals were studied with β-asymmetry detection, also yielded the spin and the magnetic moment in agreement with calculations restricted to sd-shell configurations. ^{31}Mg, however, studied with the same methods as ^{29}Mg, showed an unexpected spin and magnetic moment, which place it inside the intriguing “island of inversion.” The theory describes this state as almost purely involving two neutrons in the pf shell.

The shell-model residual interactions reproducing the “island of inversion” by a $N = 20$ shell-gap weakening and an energy gain from increased proton-neutron correlations describe well the properties of ^{31}Mg. However, there remain problems with predicting the ground state as $1/2^+$. Present theoretical attempts—including more refined residual interactions and calculations with mixing in the full pf shell—will hopefully improve the situation. At the same time, recent calculations with the antisymmetrized molecular dynamics approach already predict the $1/2^+$ level as the ground state. As for the borders of the “island,” at the beginning it was expected that an abrupt change from “normal” to intruder behavior would take place only at $N = 20$. Our result clearly shows that the change might be indeed abrupt, but—at least for Mg isotopes—it happens already at $N = 19$. For comparison, in Na ($Z = 11$) isotopes the transition nucleus is ^{29}Na with 18 neutrons and a ground state consisting of 50% intruder configurations [40]. At the same time, ^{32}Al ($Z = 13$) with 19 neutrons has a pure sd configuration, but the $N = 20$, 21 isotopes ^{33,34}Al have a mixed ground-state configuration [38,39]. More theoretical and experimental input should help to obtain a clearer picture of this interesting region of the nuclear landscape.

ACKNOWLEDGMENTS

This work is part of the Ph.D. theses of M.K. and D.Y. We thank the ISOLDE technical group for their assistance and Dr. Y. Utsuno for various discussions and his calculations on ^{29}Mg. This work was supported by the German Federal Ministry for Education and Research (BMBF) (06MZ175 and 06MZ251), the Belgian Fund for Scientific Research, Flanders (FWO), and the European Union Sixth Framework through RII3-EURONS (506065) and the Marie Curie IEF program (MEIF-CT-2006-042114).

---

[1] C. Détraz *et al.*, Nucl. Phys. **A394**, 378 (1983).
[2] N. Orr *et al.*, Phys. Lett. **B258**, 29 (1991).
[3] E. K. Warburton, J. A. Becker, and B. A. Brown, Phys. Rev. C **41**, 1147 (1990).
[4] C. Détraz *et al.*, Phys. Rev. C **19**, 164 (1979).
[5] H. Iwasaki *et al.*, Phys. Lett. **B522**, 227 (2001).
[6] T. Motobayashi *et al.*, Phys. Lett. **B346**, 9 (1995).
[7] B. Pritychenko *et al.*, Phys. Lett. **B461**, 322 (1999).
[8] V. Chiste *et al.*, Phys. Lett. **B514**, 233 (2001).
[9] H. Grawe, Lect. Notes Phys. **651**, 33 (2004).
[10] G. Neyens *et al.*, Phys. Rev. Lett. **94**, 022501 (2005).
[11] E. Kugler, Hyperfine Interact. **129**, 23 (2000).
[12] V. Fedoseyev *et al.*, Hyperfine Interact. **127**, 409 (2000).
[13] A. Müller *et al.*, Nucl. Phys. **A403**, 234 (1983).
[14] R. Neugart and G. Neyens, Lect. Notes Phys. **700**, 117 (2006).
[15] H. Kopfermann, *Nuclear Moments* (Academic Press, New York, 1968).
[16] P. Raghavan, At. Data Nucl. Data Tables **42**, 189 (1989).
[17] M. Keim *et al.*, Eur. Phys. J. A **1**, 31 (2000).
[18] W. Demtröder, *Laser Spectroscopy: Basic Concepts and Instrumentation* (Springer-Verlag, Berlin, 2003).
[19] I. Sobelman, *Atomic Spectra and Radiative Transitions* (Springer-Verlag, Berlin, 1996).
[20] W. Press *et al.*, *Numerical Recipes in C++* (Cambridge University Press, Cambridge, 2002).
[21] W. Itano and D. Wineland, Phys. Rev. A **24**, 1364 (1981).
[22] R. B. Firestone and J. Tauren, LBNL Isotopes Project Nuclear Data Dissemination Home Page, http://ie.lbl.gov/toi.html.
[23] M. Kowalska, Hyperfine Interact. **162**, 109 (2005).
[24] B. Brown and B. Wildenthal, Annu. Rev. Nucl. Part. Sci. **38**, 29 (1988).
[25] B. A. Brown and W. A. Richter, Phys. Rev. C **74**, 034315 (2006).
[26] E. Caurier and F. Nowacki, Acta Phys. Pol. B **30**, 705 (1999).
[27] E. Caurier, F. Nowacki, and A. Poves, Eur. Phys. J. A **15**, 145 (2002).
[28] J. Retamosa, E. Caurier, F. Nowacki, and A. Poves, Phys. Rev. C **55**, 1266 (1997).
[29] S. Nummela *et al.*, Phys. Rev. C **63**, 044316 (2001).
[30] F. Nowacki (private communication).
[31] E. Caurier *et al.*, Rev. Mod. Phys. **77**, 427 (2005).
[32] F. Maréchal *et al.*, Phys. Rev. C **72**, 044314 (2005).
[33] Y. Utsuno, T. Otsuka, T. Mizusaki, and M. Honma, Phys. Rev. C **60**, 054315 (1999).
[34] M. Honma, T. Otsuka, B. A. Brown, and T. Mizusaki, Phys. Rev. C **69**, 034335 (2004).
[35] T. Otsuka *et al.*, Prog. Part. Nucl. Phys. **46**, 155 (2001).
[36] T. Otsuka (private communication).
[37] Y. Utsuno (private communication).
[38] P. Himpe *et al.*, Phys. Lett. **B658**, 203 (2008).
[39] P. Himpe *et al.*, Phys. Lett. **B643**, 257 (2006).
[40] Y. Utsuno, T. Otsuka, T. Glasmacher, T. Mizusaki, and M. Honma, Phys. Rev. C **70**, 044307 (2004).
[41] A. Klein *et al.*, Nucl. Phys. **A607**, 1 (1996).

[42] W. Geithner *et al.*, Phys. Rev. C **71**, 064319 (2005).
[43] K. Shimomura *et al.*, RIKEN Annual Report **25**, 1991 (unpublished).
[44] N. Stone, At. Data Nucl. Data Tables **90**, 75 (2005).
[45] P. Baumann *et al.*, Phys. Rev. C **39**, 626 (1989).
[46] H. Mach *et al.*, Eur. Phys. J. A **25**, 105 (2005).
[47] G. Klotz *et al.*, Phys. Rev. C **47**, 002502 (1993).
[48] D. Yordanov *et al.*, Phys. Rev. Lett. **99**, 212501 (2007).
[49] I. Hamamoto, Phys. Rev. C **76**, 054319 (2007).
[50] J. Dechargé and D. Gogny, Phys. Rev. C **21**, 1568 (1980).
[51] M. Kimura, Phys. Rev. C **75**, 41302(R) (2007).